EUROfusion

WP14ER-PR(17) 18268

J Loizu et al.

Scrape-off-layer current loops and floating potential in limited tokamak plasmas

Preprint of Paper to be submitted for publication in
Journal of Plasma Physics

This work has been carried out within the framework of the EUROfusion Consortium and has received funding from the Euratom research and training programme 2014-2018 under grant agreement No 633053. The views and opinions expressed herein do not necessarily reflect those of the European Commission.

Scrape-off-layer current loops and floating potential in limited tokamak plasmas

J. LOIZU[1], J. A. MORALES[2], F. D. HALPERN[3], AND P. RICCI[4] †

[1]Max-Planck-Institut für Plasmaphysik, D-17491 Greifswald, Germany
[2] Commissariat à l'Energie Atomique, Cadarache, France
[3]General Atomics, San Diego, California, USA
[4]Swiss Plasma Center, Ecole Polytechnique Fédérale de Lausanne, Switzerland

(Received ?; revised ?; accepted ?. - To be entered by editorial office)

We investigate the question of how are plasma currents circulating and closing in the scrape-off-layer (SOL) of convection-limited tokamak plasmas. A simplified two-fluid model describes how currents must evacuate charge at the sheaths due to cross-field currents that are not divergence-free. These include turbulence-driven polarization currents and poloidally asymmetric equilibrium diamagnetic currents. The theory provides an estimate for the radial profile of the floating potential, which reveals a dipolar structure as the one observed experimentally. Simulations with a fluid turbulence code provide evidence for the predicted behaviour of currents and floating potential.

1. Introduction

Recent experiments have shown that large steady-state plasma currents to the targets establish in the scrape-off-layer (SOL) of limited tokamaks (Dejarnac *et al.* 2015; Nespoli *et al.* 2016; Tsui *et al.* 2017; Halpern *et al.* 2017). These currents are radially localized and carry large amounts of negative charge out of the plasma via the sheaths in the near-SOL. Given that essentially no charge is injected into the plasma, it must be that *no net charge* can be flowing out of the plasma in steady-state. These observations thus lead to the following fundamental question: how are currents circulating and closing in the SOL?

The answer to this question is probably one of the missing pieces of the puzzle that is the generation of the so-called *narrow heat flux feature* in the SOL (Kocan *et al.* 2015), which has recently become crucial for the design of ITER and future magnetic fusion devices (Motojima 2015) . While the sheath currents themselves are not the main direct contributors to the increased heat flux in the near-SOL (Dejarnac *et al.* 2015), the plasma potential profile resulting from the non-ambipolarity at the sheaths plays a crucial role in the description of the gradient-steepening in the near-SOL via strongly sheared $\mathbf{E}\times\mathbf{B}$ flows (Tsui 1992; Halpern & Ricci 2017).

If there were no radial cross-field currents in the SOL, then every flux-tube would be independent in terms of charge conservation. Namely, we would have that in a given flux-tube the plasma current to the targets, if any, is equal and opposite at each end of the field line. Experiments show, however, that on certain flux-tubes large equilibrium plasma currents evacuate *net charge* at the targets, and associated to that a non-zero floating potential is measured. This suggests that non-divergence-free cross-field currents must

† Email address for correspondence: joaquim.loizu@ipp.mpg.de

develop in the SOL to ensure charge conservation. Furthermore, since the plasma density radially decays in the SOL, the net positive charge that is transported by cross-field currents is most likely evacuated through the sheaths as well, perhaps in the transition between the near-SOL and the far-SOL. A somewhat equivalent picture was already realized in (Tsui 1992). In that work, however, a current circulation model was developed based on the assumption that cross-field transport was dominated by ion-neutral collisions, and the magnitude of the non-ambipolar flows established at the sheaths was predicted to *increase* with the ion-neutral collision frequency. While this model may certainly explain non-ambipolar flows in certain experiments (Strawitch & Emmert 1981), it cannot describe the recent observations made in ITER-relevant tokamak devices: the fact that the magnitude of these sheaths currents *decreases* with plasma collisionality, namely with ν^*_{SOL} (Tsui *et al.* 2017). Moreover, it has been recently shown via nonlinear SOL turbulence simulations that both the heat-flux narrow feature and the associated non-ambipolar flows arise even without accounting for the effect of neutrals (Halpern & Ricci 2017).

In this paper, we develop a simple but useful model to elucidate the question of how are currents circulating in the SOL. The model predicts that a non-zero floating potential profile with a dipolar structure appears as a natural consequence of turbulence-driven cross-field currents, and we provide estimates for its magnitude and scale. Certain of these model predictions have been been recently shown to compare well with experimental measurements (Tsui *et al.* 2017). Here we also show that numerical simulations carried out with a fluid turbulence code lend further support to the model.

2. Theory of current closure

The fundamental equation we need to solve is the one that describes the conservation of charge in the SOL, namely

$$\frac{\partial \rho}{\partial t} + \nabla \cdot \mathbf{j} = 0 \tag{2.1}$$

where ρ is the charge density and $\mathbf{j}$ is the current density. We neglect here the effect of neutrals, which may restrict the validity of the model to convection-limited regimes (Stangeby 2000). Also, we use the drift-reduced Braginskii theory (Zeiler *et al.* 1997), which may restrict the validity of the model to regimes in which the scale-lengths are larger than the ion gyroradius; this is particularly true in L-mode plasmas. In this limit, the fluid velocities of electrons and ions are, respectively, $\mathbf{v}_e = v_{\parallel e}\mathbf{b} + \mathbf{v}_{E\times B} + \mathbf{v}_{dia,e}$ and $\mathbf{v}_i = v_{\parallel i}\mathbf{b} + \mathbf{v}_{E\times B} + \mathbf{v}_{dia,i} + \mathbf{v}_{pol}$. Namely, the perpendicular velocity is expanded in terms of a small parameter, $\epsilon = \omega_{ci}^{-1}(d/dt) \sim \rho_i^2/L_\perp^2 \ll 1$, so that the $\mathbf{E}\times\mathbf{B}$ drift and diamagnetic drifts, $\mathbf{v}_{E\times B}$ and $\mathbf{v}_{dia}$, are the zeroth-order terms, and the lowest-order ion polarization drift,

$$\mathbf{v}_{pol} = \frac{\mathbf{b}}{\omega_{ci}} \times \left(\frac{\partial}{\partial t} + (\mathbf{v}_{E\times B} + v_{\parallel i}\mathbf{b}) \cdot \nabla \right) \mathbf{v}_{E\times B} \ , \tag{2.2}$$

is of order $O(\epsilon)$. Here $\omega_{ci} = eB/m_i$ is the gyrofrequency, $\rho_i = v_{thi}/\omega_{ci}$ is the gyroradius, $v_{thi} = \sqrt{T_i/m_i}$ is the thermal speed, and $L_\perp$ is the equilibrium perpendicular scale-length. The absence of the ion diamagnetic drift in the convective derivative is due to the so-called diamagnetic cancellation which arises from the lowest order term in the pressure tensor, in the large aspec-ratio limit (Ramos 2005). The electron polarization drift is of order $(m_e/m_i)O(\epsilon)$ and is neglected. Under these assumptions, Eq. (2.1) can be reduced to

$$\langle \nabla_\parallel j_\parallel \rangle_{t,\theta} + \langle \nabla \cdot \mathbf{j}_{dia} \rangle_{t,\theta} + \langle \nabla \cdot \mathbf{j}_{pol} \rangle_{t,\theta} = 0 \tag{2.3}$$

where $< \cdot >_{t,\theta}$ represents a time-average and poloidal-average,

$$\langle F \rangle_{t,\theta}\ (r) \equiv \frac{1}{2\pi} \int_0^{2\pi} \left[\frac{1}{T} \int_0^T F(r,\theta,\varphi,t) dt \right] d\theta \tag{2.4}$$

where (r, θ, φ) are toroidal coordinates and the time interval T is much larger than the time-scale of turbulence fluctuations. Writing $F(r,\theta,\varphi,t) = \langle F \rangle_{t,\theta}(r) + \tilde{F}(r,\theta,\varphi,t)$, we consider $T \gg |\tilde{F}/\partial_t \tilde{F}|$.

We now estimate the three terms in the charge-balance equation (2.3), which are the divergence of the parallel, diamagnetic, and polarization currents. This will lead to an equation for the radial profile of plasma potential, thereby providing a prediction for the profile of floating potential.

2.1. *Parallel term*

In the absence of magnetic flutter, namely in the electrostatic limit, the time-average of the divergence of the parallel current is $\langle \nabla_\parallel j_\parallel \rangle_t = \nabla_\parallel \langle j_\parallel \rangle_t$. Assuming a circular tokamak equilibrium, we then have that

$$\langle \nabla_\parallel j_\parallel \rangle_{t,\theta} = \frac{\langle j_\parallel \rangle_t^+ - \langle j_\parallel \rangle_t^-}{L_\parallel} \tag{2.5}$$

where $L_\parallel = 2\pi q R$ is the parallel connection length, $q = q(r)$ is the safety factor, and $\langle j_\parallel \rangle_t^\pm$ is the time-averaged parallel current evaluated at both sides of the limiter, referred to as *top* (+) and *bottom* (−), respectively. More precisely, these are evaluated at the entrance of the magnetic presheath (Loizu *et al.* 2012). The parallel current density is $j_\parallel = en(v_{\parallel i} - v_{\parallel e})$ and we assume that

$$\langle j_\parallel \rangle_t \approx e \langle n \rangle_t \Big(\langle v_{\parallel i} \rangle_t - \langle v_{\parallel e} \rangle_t \Big) \ . \tag{2.6}$$

In doing so, we have neglected the terms $\langle \tilde{n} \tilde{v}_\parallel \rangle_t$ with respect to the terms $\langle n \rangle_t \langle v_\parallel \rangle_t$. This is justified since, even if fluctuations correlate perfectly, we have that

$$\frac{\langle \tilde{n} \tilde{v}_\parallel \rangle_t}{\langle n \rangle_t \langle v_\parallel \rangle_t} \sim \left(\frac{\tilde{n}}{\langle n \rangle_t} \right) \left(\frac{\tilde{v}_\parallel}{c_s} \right) \ll 1 \tag{2.7}$$

because in typical SOL conditions, $\tilde{n}/\langle n \rangle_t \approx 0.05 - 1$ (Zweben *et al.* 2007) and $\tilde{v}_\parallel / c_s \approx 0.1 - 0.5$ (Hidalgo *et al.* 2003). Here $c_s = \sqrt{(T_e + T_i)/m_i}$ is the plasma sound speed. The equilibrium parallel current at the entrance of the magnetic presheath is taken as the Bohm current, namely,

$$\langle j_\parallel \rangle_t^\pm = \pm e \langle n \rangle_t^\pm \langle c_s \rangle_t^\pm \left(1 - e^{\langle \Lambda \rangle_t^\pm - \frac{e \langle \phi \rangle_t^\pm}{\langle T_e \rangle_t^\pm}} \right) , \tag{2.8}$$

where the plasma potential, ϕ, is measured with respect to the wall potential, which is taken as the zero of the potential, $\phi_{wall} = 0$. The quantity

$$\Lambda = \log \sqrt{\frac{m_i}{2\pi m_e} \frac{1}{1 + \frac{T_i}{T_e}}} \tag{2.9}$$

determines the ambipolar potential, i.e. $\langle j_\parallel \rangle_t^\pm = 0$ if and only if $e \langle \phi \rangle_t^\pm = \langle \Lambda \rangle_t^\pm \langle T_e \rangle_t^\pm$. In principle, the sheath parallel current contains an additional term mainly due to the recirculation of the diamagnetic current (Loizu *et al.* 2012), but this does not contribute to the outflow of charge since it is simply compensating the outflowing diamagnetic current (Cohen & Ryutov 1995). In practice, therefore, the contribution from the ouflowing diamagnetic current at the sheaths shall be ignored.

2.2. *Diamagnetic term*

The divergence of the diamagnetic current is

$$\nabla\cdot\mathbf{j}_{dia}=\nabla p\cdot\nabla\times\left(\frac{\mathbf{b}}{B}\right) \tag{2.10}$$

where $p=p_e+p_i$ is the total scalar plasma pressure. Assuming a large-aspect-ratio, circular magnetic equilibrium, Eq. (2.10) reduces to

$$\nabla\cdot\mathbf{j}_{dia}=\frac{2}{BR}\Big(\cos\theta\frac{1}{r}\frac{\partial p}{\partial\theta}+\sin\theta\frac{\partial p}{\partial r}\Big) \tag{2.11}$$

where R is the major radius of the tokamak. We now assume that

$$\langle\cos\theta\frac{1}{r}\frac{\partial p}{\partial\theta}\rangle_{t,\theta}\approx 0 \tag{2.12}$$

and

$$\langle\sin\theta\frac{\partial p}{\partial r}\rangle_{t,\theta}\approx-\frac{\delta p}{L_p} \tag{2.13}$$

where $L_p=|\langle p\rangle_{t,\theta}/\partial_r\langle p\rangle_{t,\theta}|$ is the equilibrium pressure scale-length, and $\delta p\approx\langle p\rangle_t^+-\langle p\rangle_t^-$ measures the poloidal asymmetry in the pressure. These assumptions are justified in Appendix A, based on the effects that $\mathbf{E}\times\mathbf{B}$ drifts and poloidally asymmetric cross-field transport have on the equilibrium pressure profile. In particular, an estimate for the pressure poloidal asymmetry is provided, showing that $\delta p/p\sim 0.1$ is expected for an inner-wall-limited plasma with ballooning-like cross-field transport. Therefore, we have that

$$\langle\nabla\cdot\mathbf{j}_{dia}\rangle_{t,\theta}\approx-\frac{2}{BR}\frac{\delta p}{L_p} \tag{2.14}$$

2.3. *Polarization term*

Turbulence simulations in tokamak SOL geometry with medium-size tokamak parameters (Halpern & Ricci 2017) revealed that the divergence of the polarization current is mainly due to the radially sheared convection of vorticity. Namely,

$$\langle\nabla\cdot\mathbf{j}_{pol}\rangle_{t,\theta}\approx\frac{e\langle n\rangle_{t,\theta}}{\omega_{ci}B^2}\Big|\frac{\partial}{\partial r}\Big\langle\tilde{\Omega}\frac{1}{r}\frac{\partial\tilde{\phi}}{\partial\theta}\Big\rangle_{t,\theta}\Big| \tag{2.15}$$

where $\tilde{\Omega}=\nabla_\perp^2\tilde{\phi}$ is the fluctuating vorticity. We now simplify this expression by making a certain number of assumptions,

$$\begin{aligned}\langle\nabla\cdot\mathbf{j}_{pol}\rangle_{t,\theta}&\approx\frac{e\langle n\rangle_{t,\theta}}{\omega_{ci}B^2}\Big|\frac{\partial}{\partial r}\Big\langle k_\perp^2k_\theta\tilde{\phi}^2\Big\rangle_{t,\theta}\Big|\\&\approx\frac{e\langle n\rangle_{t,\theta}}{k_\theta\omega_{ci}}\Big|\frac{\partial\gamma^2}{\partial r}\Big|\\&\approx\frac{e\langle n\rangle_{t,\theta}}{k_\theta\omega_{ci}}\frac{1}{RL_p}\Big|\frac{\partial\langle c_s^2\rangle_{t,\theta}}{\partial r}\Big|\end{aligned}$$

$$\approx \frac{e\langle n\rangle_{t,\theta}}{k_\theta\omega_{ci}}\frac{\langle c_s\rangle_{t,\theta}^2}{RL_pL_T}$$

$$\approx \frac{e\langle n\rangle_{t,\theta}\langle c_s\rangle_{t,\theta}}{k_\theta\langle\rho_s\rangle_{t,\theta}R}\frac{2}{5}\left(\frac{\langle\rho_s\rangle_{t,\theta}}{L_p}\right)^2 \tag{2.16}$$

where $\rho_s = c_s/\omega_{ci}$ is the ion sound Larmor radius. Here we have assumed that the saturated amplitude of the fluctuations has magnitude $\langle\tilde{\phi}^2\rangle_{t,\theta} \sim B^2\gamma^2/(k_\theta^2 k_r^2)$, where $\gamma \sim c_s/\sqrt{RL_p}$ is the linear growth rate for interchange-like modes. We also have assumed that eddies have comparable radial and poloidal wavenumbers, $k_\perp \sim k_r \sim k_\theta$ (Zweben *et al.* 2015), and have taken $L_T = (5/2)L_p$ for the equilibrium temperature scale-length. These assumptions are based on the hypothesis that (i) resistive ballooning modes are dominant, (ii) saturation of fluctuations occurs due to the gradient removal mechanism (Ricci & Rogers 2013), and (iii) there is no effect of shear flows on mode growth (which may overestimate the term). Of course, because of these assumptions a correction factor of order one may be applied in front of this term. For our purposes, however, what matters is the scaling and the order of magnitude of this term.

2.4. *Overall charge balance*

Bringing together the approximate expressions for each of the three terms in Eq. (2.3), dropping the bracket notation (all quantities are now averages), and dividing everything by $enc_s/(2\pi qR)$, we get

$$\frac{\Gamma^+}{\Gamma}(1-e^{\Lambda^+-\frac{e\phi^+}{T_e^+}})+\frac{\Gamma^-}{\Gamma}(1-e^{\Lambda^--\frac{e\phi^-}{T_e^-}})+2\pi q\Big[\frac{1}{k_\theta\rho_s}\frac{2}{5}\left(\frac{\rho_s}{L_p}\right)^2-2\frac{\delta p}{p}\left(\frac{\rho_s}{L_p}\right)\Big]\approx 0 \tag{2.17}$$

where $\Gamma = nc_s$ and $\Gamma^\pm = n^\pm c_s^\pm$. The validity of Eq. (2.17) is verified with turbulence simulations in Sec. 3. We now further simplify this expression in order to derive a simple expression for the floating potential. In the limit of a sheath-limited regime (Stangeby 2000), in which we can assume that $\Gamma^\pm \approx \Gamma/2$, $\Lambda^\pm \approx \Lambda$, and $\phi^\pm/T_e^\pm \approx \phi/T_e$, Eq. (2.17) reduces to

$$1-e^{-\frac{V_f}{T_e}}+2\pi q\Big[\frac{1}{k_\theta\rho_s}\frac{2}{5}\left(\frac{\rho_s}{L_p}\right)^2-2\frac{\delta p}{p}\left(\frac{\rho_s}{L_p}\right)\Big]\approx 0 \tag{2.18}$$

where $V_f = e\phi - \Lambda T_e$ is the floating potential. Solving for V_f, we have that

$$V_f \approx -T_e\ln(1+\Delta) \tag{2.19}$$

with

$$\Delta = 2\pi q\Big[\frac{1}{k_\theta\rho_s}\frac{2}{5}\left(\frac{\rho_s}{L_p}\right)^2-2\frac{\delta p}{p}\left(\frac{\rho_s}{L_p}\right)\Big]\,. \tag{2.20}$$

The function Δ determines whether there are electron currents to the sheath ($\Delta > 0$), no sheath currents ($\Delta = 0$), or ion currents to the sheath ($\Delta < 0$). Here L_p and $\delta p/p$ are seen as functions of the radius, r, and so $\Delta = \Delta(r)$. The first term in Eq. (2.20) is the polarization current contribution due to turbulent fluctuations, and the second term is the diamagnetic current contribution, which is only non-zero due to finite magnetic curvature and gradients, and whose poloidal average does not vanish when pressure asymmetries are present. In Appendix A, we estimate that typically $\delta p/p \sim 0.1$ is expected in inner-wall-limited plasmas with ballooning-like cross-field transport. These numbers are also confirmed in SOL turbulence simulations (see Sec. 3). Also, we typically expect $k_\theta\rho_s \sim 0.1$

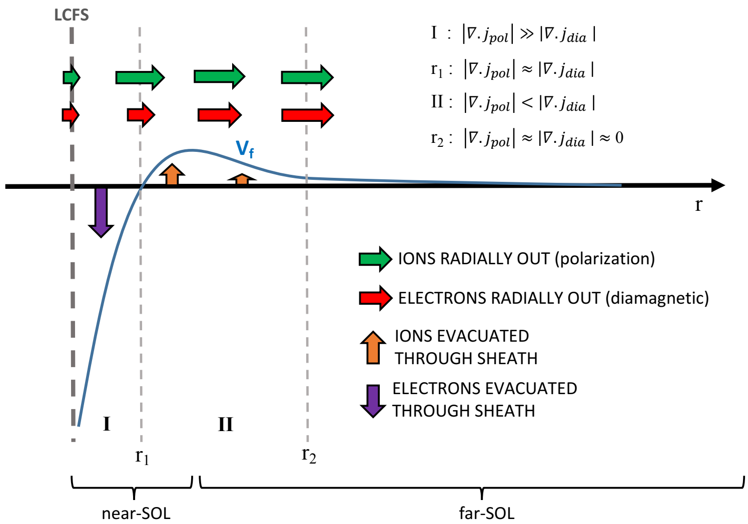

FIGURE 1. Schematic view of the current circulation in the SOL.

(Mosetto *et al.* 2013). We can thus estimate the ratio of the two terms in Eq. (2.20) as $\Delta_{pol}/\Delta_{dia} \sim 20\rho_s/L_p$. In the near-SOL, L_p is of the order of a few mm (Tsui *et al.* 2017), thus $\Delta_{pol} > \Delta_{dia}$; while it becomes of the order of a few cm in the far-SOL, and thus $\Delta_{pol} < \Delta_{dia}$. Hence we expect that $\Delta > 0$ in the near-SOL and $\Delta < 0$ in the far-SOL.

The picture of how currents circulate in the SOL emerges as follows (Figure 1). Radially increasing polarization currents push ions radially outward in the near-SOL; the sheath must then evacuate electrons to compensate the loss of charge ($V_f < 0$, region I in Fig.1). As L_p becomes larger, the increase in polarization current is reduced; also, pressure asymmetries may have built up and produce diamagnetic currents that push electrons radially outward; the sheath is then relieved from the task of compensating ($V_f \approx 0$, $r = r_1$ in Fig.1). The polarization contribution, $\Delta_{pol} \sim (\rho_s/L_p)^2$, dies out faster than the diamagnetic contribution, $\Delta_{dia} \sim (\rho_s/L_p)$, thus leading to an effective outward push of negative charge; the sheath must now evacuate ions to compensate ($V_f > 0$, region II in Fig.1). Finally, both contributions cancel each other once again because the divergence of each current dies away ($V_f \approx 0$, $r = r_2$ in Fig.1).

3. SOL turbulence simulations

The GBS code (Ricci *et al.* 2012; Halpern *et al.* 2016) is used to simulate the SOL electrostatic turbulence in an inner-wall-limited tokamak plasma configuration of relatively small size, $R/\rho_s = 500$; aspect ratio $R/a = 4$; normalized plasma resistivity $\nu = e^2 n_e c_s/(m_i \sigma_\| R) = 0.1$, where $\sigma_\|$ is the Spitzer conductivity; mass ratio $m_i/m_e = 200$; safety factor $q = 4$; and only with an open-field-line region. The Boussinesq approximation is relaxed to ensure an accurate conservation of charge (Halpern *et al.* 2016) and a complete set of boundary conditions at the magnetic presheath entrance is used (Loizu *et al.* 2012).

We consider two cases: cold ions ($\tau = 0$) and warm ions ($\tau = 2$). For each case, we check the validity of the approximate charge-balance equation derived in Sec. 2, namely Eq. (2.17), by comparing the three terms corresponding to the parallel, diamagnetic, and

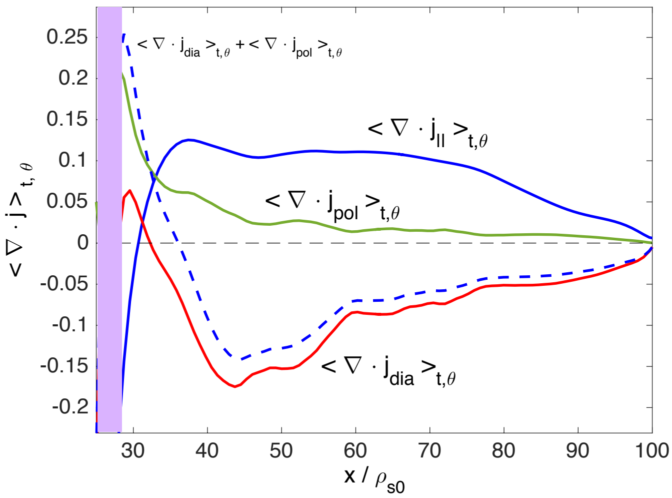

FIGURE 2. Charge-balance terms computed from the different contributions in Eq. (2.17) and using the equilibrium quantities obtained from GBS simulations with $\tau = 0$. The vertical violet stripe indicates the extent of the density and heat source in the simulations. From Eq. (2.17), the dashed-blue curve is expected to approximately balance the solid blue line.

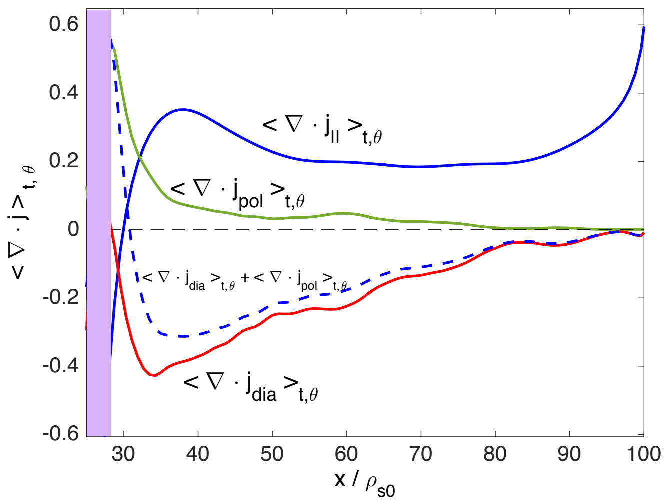

FIGURE 3. Same as Fig. 2 but with $\tau = 2$.

polarization contributions, expressed analytically as a function of equilibrium quantities. Figures 2 and 3 show these different contributions as a function of the radial coordinate in the SOL. We observe that the three terms balance each other relatively well, especially in the $\tau = 2$ case. In both cases, the parallel term is balanced first by the polarization term (near-SOL), and then by the diamagnetic term (far-SOL). The maximum of the pressure asymmetry, $\delta p/p$, is ≈ 0.1 for the $\tau = 0$ case and ≈ 0.25 for the $\tau = 2$ case. This is in agreement with the magnitude and sign estimated in the Appendix A.

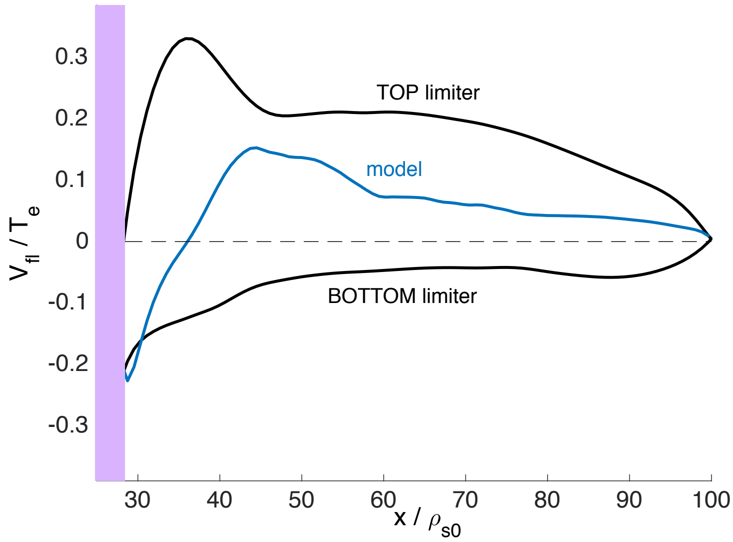

FIGURE 4. Radial profile of floating potential obtained from GBS (black curves) and from the model (blue curve), Eq. (2.19), for the case $\tau = 0$. The vertical violet stripe indicates the extent of the density and heat source in the simulations.

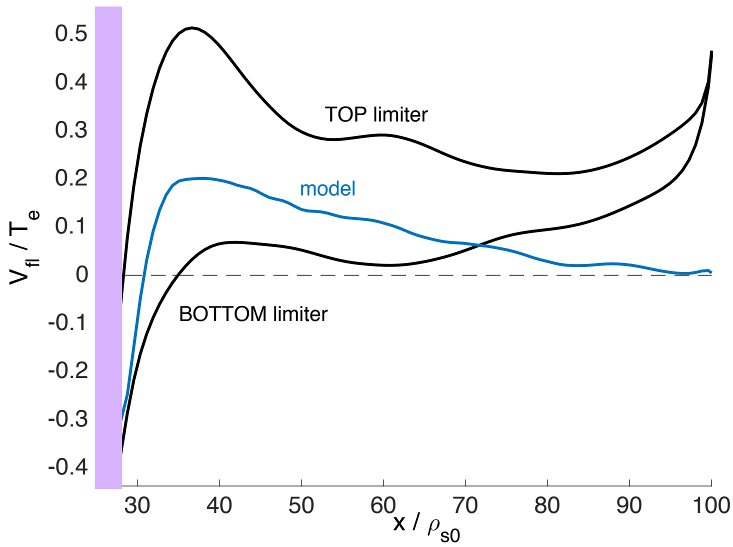

FIGURE 5. Same as Fig. 4 but with $\tau = 2$.

The validity of Eq. (2.18), or equivalently, the predicted profile of floating potential, Eq. (2.19), relies on the assumption that V_f is the same on both sides of the limiter. Figures 4 and 5 show that this is not exactly true in the simulations, especially in the $\tau = 0$ case. Nevertheless, the predicted profile of $V_f(r)$ does lie in between $V_f^+(r)$ and $V_f^-(r)$, and shows a dipolar structure. This structure is in agreement with the picture of current circulation proposed in Sec. 2.

4. Conclusion

The theory of current circulation developed herein is consistent with turbulence simulations but the floating potential cannot be assumed to be poloidally symmetric. Improving the predictions for $V_f(r)$ may require a more detailed study of poloidal asymmetries (Loizu *et al.* 2014). Nevertheless, the model predicts that a "V_f-hump" appears as a consequence of two competing non-divergence-free cross-field currents, namely (1) turbulence-driven polarization currents and (2) poloidally asymmetric diamagnetic currents. A relatively simple expression for $V_f(r)$, Eq. (2.19), has been derived that could be used for the interpretation of experimental measurements. In fact, the dependence of the amplitude of this hump, $\max|V_f(r)|$, on the adimensional parameter ν^*_{SOL} was recently shown to be consistent with the predictions of the model (Tsui *et al.* 2017). In fact, the value of ν^*_{SOL} was experimentally varied by scanning I_p, namely the toroidal plasma current. The amplitude of the "V_f-hump" was observed to increase with I_p but only above a certain threshold, and these features were reproduced by the model described herein (see Fig. 11 of (Tsui *et al.* 2017)). The reason is that I_p significantly modifies the electron temperature profile, $T_e(r)$, in the SOL, thereby altering the values of ρ_s/L_p appearing in the model.

This paper provides a first detailed look at how currents circulate and close in the SOL and proposes a simple expression for the radial profile of the floating potential. Furthermore, this work may guide future investigations seeking to develop a more detailed understanding of the formation of the narrow heat-flux feature as well as that of a poloidally asymmetric floating potential profile.

We acknowledge useful discussions with C. Tsui, J. Boedo, C. Wersal, and F. Riva. This work has been partly carried out in the framework of the EUROfusion Consortium and has received funding from the Euratom research and training programme 2014-2018 under Grant Agreement No. 633053. The views and opinions expressed herein do not necessarily reflect those of the European Comission. The material in this paper is also partly based upon work supported by the U.S. Department of Energy, Office of Science, Office of Fusion Energy Sciences, Theory Program, under Award No. DE-FG02-95ER54309.

Appendix A

Here we estimate the effect of poloidal drifts (in general both $\mathbf{E}\times\mathbf{B}$ and diamagnetic) on the pressure poloidal profile and in particular we estimate the term $\delta p/p$.

The ion continuity equation in a flux tube can be written as

$$\frac{\partial}{\partial y}(nV_y) = S_p \tag{A 1}$$

where $y = r\theta$ is the poloidal coordinate, V_y is the ion poloidal velocity (which is the sum of the projected parallel velocity and the poloidal drifts), and S_p is the plasma volumetric source in the flux-tube, which is for example determined by the divergence of the turbulent cross-field transport. This leads to

$$n(y) = \frac{\int_{y_0}^{y} S_p dy}{V_y(y)} \tag{A 2}$$

where y_0 is the location at which $V_y(y_0) = 0$. We consider four cases:

(1) $S_p = S_0$ and $V_y = (2\alpha c_s/L)y$;

(2) $S_p = S_0$ and $V_y = (2\alpha c_s/L)y + v_D$;

(3) $S_p = S_0(1 - y^2/l^2)$ and $V_y = (2\alpha c_s/L)y$;

(4) $S_p = S_0(1 - y^2/l^2)$ and $V_y = (2\alpha c_s/L)y + v_D$.

Here $L = 2\pi qR$, $y \in (-y_m, y_m)$, $y_m = L/2$, α is the pitch angle of the magnetic field, v_D is the sum of poloidal drifts (which is assumed constant), and $l \gtrsim L$ is the scale length of variation of the source, which mimics a "ballooning-like" transport with maximum amplitude half-way between the two targets. Case (4) is thus implicitly assuming an inner-wall-limited plasma. For the case (1), $y_0 = 0$ and we simply get

$$n(y) = \frac{S_0 L}{2\alpha c_s} \equiv n_0 \ . \tag{A 3}$$

For the case (2), $y_0 = -v_E L/(2\alpha c_s)$ and we still get $n(y) = n_0$. That implies that a constant poloidal drift alone does not produce an asymmetry in the density. For the case (3), $y_0 = 0$ and we get

$$n(y) = n_0 \frac{\int_0^y (1 - y^2/l^2) dy}{y} = n_0 \left(1 - \frac{y^2}{3l^2}\right) \ . \tag{A 4}$$

Finally, for the case (4), $y_0 = -v_E L/(2\alpha c_s)$ and we get

$$n(y) = n_0 \frac{\int_{y_0}^y (1 - y^2/l^2) dy}{y - y_0} = n_0 \left(1 - \frac{1}{3l^2}(y^2 + y y_0 + y_0^2)\right) \ . \tag{A 5}$$

Therefore there is only a density asymmetry, Eq. (A 5), if the poloidal flow is asymmetric *and* the source is not constant. We can now estimate the density asymmetry for the last case,

$$\frac{n^+ - n^-}{n_0} = -\frac{2 y_0 y_m}{3l^2} = \frac{1}{6}\frac{v_D}{\alpha c_s}\left(\frac{L}{l}\right)^2 \tag{A 6}$$

providing an estimate $\delta n/n < 1/6$, thus $\delta n/n \sim 0.1$ for $v_D \lesssim \alpha c_s$ and $l \gtrsim L$. A better estimate for Eq. (2.13) comes from evaluating directly the integral

$$\frac{1}{2y_m}\int_{-y_m}^{y_m} \sin\left(\frac{y\pi}{y_m}\right) n(y)\, dy = -n_0 \frac{y_m y_0}{3\pi l^2} = n_0 \frac{1}{12\pi}\frac{v_D}{\alpha c_s}\left(\frac{L}{l}\right)^2 \tag{A 7}$$

which leads to $\delta n/n \sim 1/36 \sim 0.03$. Assuming a similar estimate for $\delta T/T$, we thus expect $\delta p/p \sim 0.03(2 + \tau) \sim 0.1$, where $\tau = T_i/T_e$. Also, in this case we have that

$$\frac{1}{2y_m}\int_{-y_m}^{y_m} \cos\left(\frac{y\pi}{y_m}\right)\frac{\partial n(y)}{\partial y}\, dy = 0 \tag{A 8}$$

which lends support to Eq. (2.12).

REFERENCES

Cohen, Ronald H & Ryutov, Dmitri D 1995 Plasma sheath in a tilted magnetic field : Closing of the diamagnetic currents ; effect on plasma convection. *Physics of Plasmas* **2** (6).

Dejarnac, R, Stangeby, P C, Goldston, R J, Gauthier, E, Horacek, J, Hron, M, Kocan, M, Komm, M, Panek, R, Pitts, R A & Vondracek, P 2015 Understanding narrow SOL power flux component in COMPASS limiter plasmas by use of Langmuir probes. *Journal of Nuclear Materials* **463**, 381–384.

Halpern, Federico D, Labombard, Brian, Terry, James L & Zweben, Stewart J 2017 Outer midplane scrape-off layer profiles and turbulence in simulations of Alcator C-Mod inner-wall limited discharges. *Physics of Plasmas* **24**.

Halpern, F D & Ricci, P 2017 Velocity shear , turbulent saturation , and steep plasma gradients in the scrape-off layer of inner-wall limited tokamaks. *Nuclear Fusion* **57**.

Halpern, F D, Ricci, P, Jolliet, S, Loizu, J, Morales, J, Mosetto, A, Musil, F, Riva, F, Tran, T M & Wersal, C 2016 The GBS code for tokamak scrape-off layer simulations. *Journal of Computational Physics* **315**, 388–408.

Hidalgo, C, Gonc, B, Silva, C, Pedrosa, M A, Erents, K, Hron, M & Matthews, G F 2003 Experimental Investigation of Dynamical Coupling between Turbulent Transport and Parallel Flows in the JET Plasma-Boundary Region. *Physical Review Letters* **91** (6).

Kocan, M, Pitts, R A, Arnoux, G, Balboa, I, de Vries, P C, Dejarnac, R, Furno, I, Goldston, R J, Gribov, Y., Horacek, J, Komm, M, Labit, B, LaBombard, B, Lasnier, C. J., Mitteau, R, Nespoli, F, Pace, D, Panek, R, Stangeby, P C, Terry, J L, Tsui, C K & Vondracek, P 2015 Impact of a narrow limiter SOL heat flux channel on the ITER first wall panel shaping. *Nuclear Fusion2* **55** (033019).

Loizu, J., Ricci, P., Halpern, F. D. & Jolliet, S. 2012 Boundary conditions for plasma fluid models at the magnetic presheath entrance. *Physics of Plasmas* **19** (12).

Loizu, J., Ricci, P., Halpern, F. D., Jolliet, S. & Mosetto, A. 2014 Effect of the limiter position on the scrape-off layer width, radial electric field and intrinsic flows. *Nuclear Fusion* **54** (8), 083033.

Mosetto, Annamaria, Halpern, Federico D., Jolliet, S??bastien, Loizu, Joaquim & Ricci, Paolo 2013 Turbulent regimes in the tokamak scrape-off layer. *Physics of Plasmas* **20** (9).

Motojima, O 2015 The ITER project construction status. *Nuclear Fusion* **104023**.

Nespoli, F, Furno, I, Halpern, F D, Labit, B, Loizu, J, Ricci, P & Riva, F 2016 Non-linear simulations of the TCV Scrape-Off Layer. *Nuclear Materials and Energy* **0**, 1–4.

Ramos, J J 2005 General expression of the gyroviscous force. *Physics of Plasmas* **12**.

Ricci, P, Halpern, F D, Jolliet, S, Loizu, J, Mosetto, A, Fasoli, A, Furno, I & Theiler, C 2012 Simulation of plasma turbulence in scrape-off layer conditions: the GBS code, simulation results and code validation. *Plasma Physics and Controlled Fusion* **54** (12), 124047.

Ricci, Paolo & Rogers, B N 2013 Plasma turbulence in the scrape-off layer of tokamak devices. *Physics of Plasmas* **20**.

Stangeby, Peter C 2000 *The Plasma Boundary of Magnetic Fusion Devices*. IOP Publishing.

Strawitch, C M & Emmert, G A 1981 NON-AMBIPOLAR TRANSPORT IN A MAGNETIC DIVERTOR. *Nuclear Fusion1* **21**.

Tsui, C K, Boedo, J A, Halpern, F D, Loizu, J, Nespoli, F, Horacek, J, Labit, B, Morales, J, Reimerdes, H, Theiler, C, Coda, S, Duval, B P, Furno, I, Team, T C V, Team, Eurofusion M S T, Tsui, C K, Boedo, J A, Halpern, F D, Loizu, J, Nespoli, F, Horacek, J & Labit, B 2017 Poloidal asymmetry in the narrow heat flux feature in the TCV scrape-off layer. *Physics of Plasmas* **24**.

Tsui, H Y W 1992 Formation of a velocity shear layer in confined plasmas: Formation of a velocity shear layer in confined plasmas. *Physics of Plasmas* **4**.

Zeiler, A, Drake, J F & Rogers, B 1997 Nonlinear reduced Braginskii equations with ion thermal dynamics in toroidal plasma. *Physics of Plasmas* **4**.

Zweben, S J, Boedo, J A, Grulke, O, Hidalgo, C, LaBombard, B, Maqueda, R J, Scarin, P & Terry, J L 2007 Edge turbulence measurements in toroidal fusion devices. *Plasma Physics and Controlled Fusion* **49**.

Zweben, S J, Davis, W M, Kaye, S M, Myra, J R, Bell, R E, Leblanc, B P, Maqueda, R J, Munsat, T, Sabbagh, S A, Sechrest, Y, Stotler, D P & NSTX 2015 Edge and SOL turbulence and blob variations over a large database in NSTX. *Nuclear Fusion* **55**.